Adsorption (2015) 21:283–305
DOI 10.1007/s10450-015-9670-z

Modelling and optimization of hybrid PSA/membrane separation processes

Dragan D. Nikolić[1] · **Eustathios S. Kikkinides**[1]

Received: 10 July 2013 / Revised: 1 April 2015 / Accepted: 9 April 2015 / Published online: 28 April 2015

Abstract The present work proposes a modelling and optimization framework for hybrid pressure swing adsorption (PSA) and membrane processes for gas separations. The hybrid PSA/membrane scheme has been applied on the process of hydrogen production from steam methane reformer off gas. Three different hybrid separation schemes have been considered and analyzed. Maximum overall hydrogen recovery has been achieved for given minimum requirements in product purity, while optimizing various PSA and membrane operating and design parameters: the number of adsorption columns, PSA cycle configurations, the number of pressure equalizations/co-current depressurization steps, multiple adsorbent layers, PSA and membrane feed pressure, purge-to-feed ratio, bed length, carbon-to zeolite ratio, membrane area, thickness, and support thickness. The optimization results have been compared to the optimization results of the PSA only case and the benefits of hybrid separation systems have been assessed in terms of the improvements in the overall hydrogen recovery ($\sim$2 %), reduction of adsorption beds size (up to 46 %), concentration of the carbon dioxide and carbon monoxide captured in a separate stream (up to 76 %), and reduction of the carbon dioxide content in the waste gases (up to 74 %).

Keywords Hybrid processes · Pressure swing adsorption · Porous membranes · Gas separations · Modeling · Optimization

List of symbols

$A_{membrane}$	Area of the membrane (m^2)
a_V	Specific area (m^2/m^3)
b	Langmuir isotherm parameter (m^3/mol)
C	Gas phase molar concentration of species i (mol/m^3)
C_i^{in}	Gas phase molar concentration of species i at the membrane inlet (mol/m^3)
C^p	Molar concentrations of gas phase in particles (mol/m^3)
c_p	Heat capacity (J/(kg K))
C_v	Gas valve constant
D	Bed diameter (m)
D_e	Effective diffusivity coefficient (m^2/s)
D_m	Molecular diffusion coefficient (m^2/s)
D_s	Surface diffusion coefficient (m^2/s)
D_z	Axial dispersion coefficient (m^2/s)
$\mathcal{Đ}_i$	Stefan Maxwell diffusivity of species i (m^2/s)
$\mathcal{Đ}_{ij}$	Stefan Maxwell diffusivity (molecule–molecule interactions) (m^2/s)
$\mathcal{Đ}_i^s$	Stefan Maxwell surface diffusivity of species i (m^2/s)
$\mathcal{Đ}_{ij}^s$	Stefan Maxwell surface diffusivity (sorbate–sorbate interactions) (m^2/s)
D_z	Axial dispersion coefficient (m^2/s)
F	Molar flowrate (mol/s)
ΔH_{ads}	Heat of adsorption (J/mol)
L	Bed or membrane unit length (m)
MW	Molecular weight (kg/mol)
N_{comp}	Number of components (–)
N_i	Molar flux, mol/(m^2 s)

✉ Eustathios S. Kikkinides
kikki@cperi.certh.gr; kikki@uowm.gr;
http://www.mech.uowm.gr

[1] Department of Mechanical Engineering, University of Western Macedonia, Sialvera & Bakola Str., 50100 Kozani, Greece

P	Total pressure (Pa)
p_i	Partial pressure of species i (Pa)
Q	Adsorbed amount (mol/kg)
Q^*	Adsorbed amount in equilibrium state with gas phase (in the mixture) (mol/kg)
Q_m	Langmuir isotherm parameter (mol/kg)
q_i^{sat}	Monolayer saturation capacity of species i (mol/kg)
q_i	The amount adsorbed of species i (mol/kg)
r	Radial domain
R_p	Particle diamater (m)
R_{bed}	Bed radius (m)
R	Ideal gas constant (J/(K mol))
T	Temperature (K)
T^p	Temperature of particles (K)
u	Interstitial velocity (m/s)
u^{in}	Interstitial velocity at the membrane inlet (m/s)
x	Molar fraction in gas phase (–)
z	Axial domain
Z	Compressibility factor (–)

PSA operating steps

PressCC	Counter-current pressurization step
Ads	Adsorption step
PEQ1, *PEQ2*, *PEQ3*	Pressure equalization steps
CoCD	Co-current depressurization step
Blow	Counter-current blowdown step
Purge	Counter-current purge step

Greek letters

δ_m	Membrane thickness (m)
δ_s	Support layer thickness (m)
ε	Adsorbent porosity (–)
ε_{bed}	Adsorbent bed porosity (–)
ε_p	Porosity of particles (–)
γ	Activity coefficient (–)
Γ	Thermodynamic factor (–)
θ	Fractional coverage (–)
θ_m	Membrane stage cut (–)
λ	Thermal conductivity (J/(m K))
λ^p	Thermal conductivity of particles (J/(m K))
μ	Viscosity (Pa s)
μ_i	Chemical potential of species i (J)
ρ	Density (kg/m^3)
ρ^p	Density of the particles (kg/m^3)
τ	Time (s)
τ_{cycle}	PSA cycle time (s)

Abbreviations

PSA	Pressure swing adsorption
SMROG	Steam methane reformer off gas
IAS	Ideal adsorption solution theory
RAS	Real adsorption solution theory
CBMC	Configurational-bias Monte-Carlo

1 Introduction

Adsorption and membrane systems have become highly important gas separation technologies in chemical manufacturing, petroleum and natural gas refining and new clean energy concepts. The importance of these technologies is evident by their application in the production of over 41 million tons/year of hydrogen and 100 million tons/year of oxygen worldwide (Ritter and Ebner 2007).

Pressure swing adsorption (PSA) has attracted increasing interest because of its low energy requirements as well as low capital investment costs in comparison to traditional separation processes such as cryogenic distillation (Ruthven 1984; Yang 1987). PSA is able to produce high purity gases at high recovery; however, capital costs and energy requirements of PSA systems are still considerably high because modern industrial PSA units typically utilize layered beds containing up to four adsorbents and, depending on the production volume, anywhere between four and sixteen beds.

Within the current state-of the-art, membrane systems offer low energy consumption, significantly lower investment costs, and ease of operation (Grol 2009). Low selectivity, however, makes problematic the production of high purity gases. If it was feasible to combine the reliable PSA technology, able to produce high purity gases with the low cost membrane systems this could lead to a substantial performance improvement, both in terms of energy requirements and overall product recovery. The additional attainable benefits are the lower overall capital costs (by decreasing the size or number of adsorption beds) and a reduced negative impact on the environment (by removing the most common pollutants, carbon monoxide and carbon dioxide).

Hybrid units can be seen as multifunctional equipment, one that couples and uncouples elementary transport, reaction and separation processes. This flexibility is used to increase productivity or selectivity for the desired product and to facilitate the separation of by-products. There are many separation processes involving hybrid unit operations. For instance, the concept of reactive or catalytic distillation has been commercialized successfully in petroleum processing and manufacturing of chemicals where reactive distillation is often employed. These hybrid units have been used to help to achieve higher conversions and yields in chemical reactors compared to conventional reactor configurations. However, the modelling and simulation of hybrid PSA/membrane separation systems has received rather limited attention in the open literature compared to modelling of PSA and membranes. Although there is some published work on the development of hybrid PSA/membrane separation systems these are seldom about

common industrial applications. Most of the works available in the literature are related to the hydrogen production and purification from various chemical and petrochemical sources (Ritter and Ebner 2007). Other example of using hybrid PSA/membrane schemes focus on the production of oxygen and nitrogen from air for on-board aircraft applications where bulk separation by membrane is followed by a purification stage by adsorption (Zolandz and Fleming 1992). There are also numerous patents that have been granted for applications such as helium recovery, hydrogen purification, acid gas removal and nitrogen production.

A successful hybrid PSA/membrane separation process has to exploit the most important features of these two technologies. To date, membrane technology is not mature enough to provide high selectivity. Thus, product purity is at a lower standard compared to PSA. However, membranes offer high fluxes, low energy consumption, possibility for continuous operation, lower investment costs and ease of operation. On the other hand, PSA is capable of producing very pure gases with high recovery rates, albeit at a higher capital investment cost and complex operation, confounded by the large number of time-dependent variables and intricate bed interconnections. By combining these two technologies, it may be possible to retain the high product purity, higher recovery and at significantly lower operating costs. For hydrogen production, waste gases of a higher calorific value, lower carbon monoxide and carbon dioxide concentrations would be a separation target.

Membrane permeation and PSA are two widely used processes for gas separation and very often considered to be alternatives or complements to the more conventional cryogenic separation process. Membrane separation is based on the difference in the rate of permeation through a membrane, while adsorption separation depends on the difference in either the rate or the equilibrium of an adsorbent. Membrane gas separation is pressure driven and normally operates continuously, whereas PSA is a cyclic process, in which beds undergo a sequence of adsorption at a high pressure and desorption at a reduced pressure, thereby making it suitable for processing a gas mixture in a continuous fashion. A concise comparison between PSA and membrane processes is given by Ruthven (1994).

In broad terms, gas permeation using current membrane technology is less selective than adsorption. Hence, membrane processes are very efficient for bulk separations whereas PSA is suitable for achieving higher purities. There are common commercial applications of hybrid process schemes combining membrane and PSA as outlined in Zolandz and Fleming (1992) for the production of O_2 and N_2 from air for aircrafts where bulk separation by membrane is followed by PSA for further purification. Another example is presented by Mercea and Hwang (1994) that studied oxygen production from air by PSA on zeolite followed by oxygen purification by a membrane. In addition, several hybrid configurations have been proposed in international patents for various applications. Those hybrid schemes can be simply classified into two categories: membrane followed by PSA, and PSA followed by membrane. In the first case, the membrane is mainly used for bulk separation and the concentrated product stream from membrane is fed to PSA for purification. If high purity is not demanded, the less concentrated stream from membrane can be fed to PSA to increase recovery. In the second case, the waste gas from PSA is fed to membrane to increase recovery, and the waste gas from membrane can be used to purge the adsorption beds.

Feng et al. (1998) proposed a novel process that incorporates membrane permeation into a PSA process. In the proposed integrated permeation/adsorption system pressure is changing as the permeation proceeds with time contrary to traditional membrane processes where pressures have been kept constant. Two configurations were considered: (a) membrane-assisted feed gas pressurization, and (b) membrane-assisted co-current depressurization. A bench scale unit was assembled and tested for hydrogen purification. It was shown that both product purity and recovery could be improved using the integrated process, compared to the simple adsorption process, particularly when the feed gas mixture contained impurities that were difficult to be removed by adsorption.

Sircar et al. (1999) evaluated experimentally the separation performance of a hybrid PSA–selective surface flow membrane process to produce a hydrogen enriched gas from the steam methane reformer off gas (SMROG). These authors analysed the operating steps where hydrogen losses can occur and identified the counter-current depressurization and counter-current purge as the critical points. Two different schemes to integrate the membrane with a PSA process were studied. In both cases the membrane was attached to the low pressure waste gases from the PSA unit and the waste gases compressed to a working pressure of 3 atm. However, one scheme uses the entire waste gas from the PSA process while the other scheme first fractionates waste gases and uses the hydrogen rich portion as an input to the membrane. The retentate stream from the membrane was recycled (mixed with the fresh PSA feed) while the permeate stream was used as a fuel gas. The results indicate that the integrated process can increase the net hydrogen recovery up to 7 %.

Esteves and Mota (2002) developed a hybrid gas separation process, designed and optimized for cyclic steady-state operation in terms of product purity and recovery. The feasibility of the proposed integrated process was assessed by conducting parametric studies on the

effect of various operating parameters on the separation performance. Furthermore the same authors developed a novel PSA/membrane scheme for gas separation, which covers both cooperative and opposing regions of the selectivity for the two stand-alone units (Esteves and Mota 2007). One hybrid scheme, denoted 'A' is applicable when the more permeable component is the least adsorbed one, whereas the 'B' hybrid process is suitable when the more permeable component is also the more adsorbed one. The 'A' scheme was thoroughly evaluated for H_2/CH_4 separation on activated carbon and a polysulfone membrane with a typical selectivity H_2/CH_4 of 35. The membrane works as a pre-bulk separation unit and is coupled to the intrinsically dynamic periodic operation of the PSA in a way that the operating pressure of the PSA unit is used as the driving force for permeation. In contrast to a conventional PSA process, adsorption beds for the integrated system are fed with a varying-composition gas stream, initially rich in the more permeable but less adsorbed component, which is progressively enriched in the other component having opposite behaviour. The hybrid process behaviour was analyzed and compared with the conventional PSA unit. The effect of various operating parameters, such as permeation throughput, total feed amount per cycle, purge-to-feed ratio, and adsorption and blowdown pressures, is assessed through detailed process simulation. The simulation results show that the inclusion of a membrane module into the cyclic adsorption process improves the separation performance when compared to stand-alone PSA. Depending on the values of the operating parameters, the integrated cycle gives H_2 and CH_4 products with purities within the ranges of 83–97 and 81–99 %, respectively. The product recoveries obtained are in the ranges of 77–99 % for H_2 and 81–98 % for CH_4. The results presented suggested that a pre-established PSA process, already in operation, could be advantageously coupled with a suitable membrane module, according to one of the proposed schemes, to enhance product purity and recovery. Whether the obtained improvements are large enough to overcome capital and extra operating costs for a given separation, must be assessed on a case by case basis.

An important conclusion drawn from these works is that the membrane permeation can be an effective aid in the pressurization and high-pressure adsorption steps of a typical PSA process. The results also indicate the feasibility of incorporating membrane permeation into the blowdown step of the PSA cycle, so that the operating pressure range available from the PSA can be used as the driving force for permeation. Therefore, a complete understanding of these hybrid processes for gas separation is crucial, mostly because of the increasing benefit in product quality, plant minimization, environmental impact, and energetic cost reduction.

2 Modelling and optimization framework

2.1 Pressure swing adsorption (PSA)

PSA is a typical multi-scale process that includes the proper interconnection of several adsorbent beds by gas valves. Each bed contains one or more adsorbent layers, while each layer consists of adsorbent particles packed into the bed. Finally adsorbent particles have a porous structure of its own, which may be often bidisperse, as in the case of zeolite adsorbents, made of zeolite crystallites stacked together with the use of a proper binding agent (Farooq and Ruthven 1989). Thus, the mathematical modelling of a PSA process has to take into account the simultaneous mass, heat and momentum balances at adsorbent bed and adsorbent particle level, gas–solid phase equilibrium, transport and thermo-physical properties of the fluids and a complicated set of boundary conditions for each operating step (due to a knotty nature of adsorbent bed connections). The resulting model equations form a complex set of coupled partial differential and algebraic equations at different scales: PSA flowsheet with bed configurations, adsorbent bed, adsorbent particle and in certain situations even at the molecular level. In order to deal with such a complex system it is necessary to build–up a hierarchical system of mathematical models each describing particular scale in a PSA process. Therefore, as far as this work is concerned the following scales exist:

- Multi-bed PSA flow-sheet
- Adsorption bed
- Adsorbent layer
- Adsorbent particle

An illustration of the various scales considered in the present PSA model is shown in Fig. 1. The developed PSA multi-bed configuration schemes and model equations employed in the present study are the same with those detailed our published work (Nikolic et al. 2008, 2009). A summary of the model equations and appropriate boundary conditions employed in the present case are given in Table 1.

The State Transition Network (STN) algorithm proposed by Nikolic et al. (2009) to develop appropriate multi-bed configurations by proper opening and closing of the valves at each bed inlet and outlet, is employed in the present study. States are represented by operating steps (that is an adsorbent bed can be in one of the operating states such as pressurization, adsorption, purge etc.); inputs are the time elapsed in the process, the time within the current cycle and several input parameters known a priory at the time of execution. Each state (the operating step) includes a set of boundary conditions and gas valves states (open/closed). A deterministic Finite State Machine (FSM) is implemented where the next possible state is uniquely

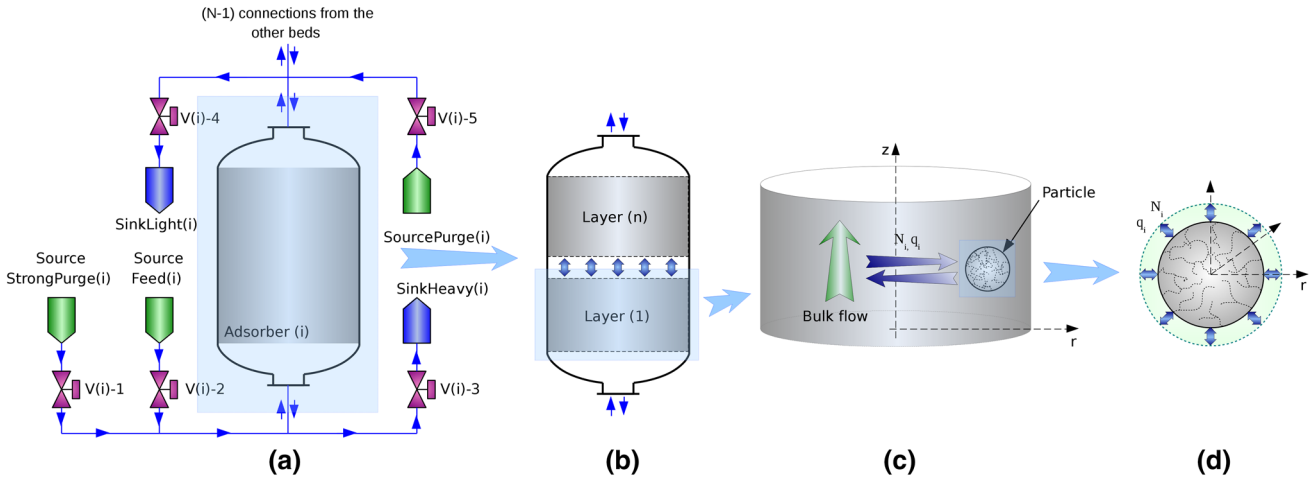

Fig. 1 The concept of multiscale modelling in a PSA process. **a** Multi-bed flow sheet, **b** adsorption bed, **c** adsorbent layer and **d** adsorbent particle

determined for a given (current) state and input values. State transitions are decisions when the state change should occur (based on the input values). This way, it is possible to control the execution of the process by specifying few parameters such as the number of beds, the sequence of steps in one bed, the number of pressure equalization steps, and the start time and duration of each step. Further details on the STN method are given elsewhere (Nikolic et al. 2009).

2.2 Membrane modelling

Theoretical approaches for modelling diffusion in microporous structures generally fall into two different categories: a kinetic approach and an approach based on irreversible thermodynamics. The kinetic approach is based on random walk models and/or transition state theory appropriately modified to account for several additional phenomena such as multilayer adsorption, surface heterogeneity and energy barriers (Yang et al. 1973; Chen and Yang 1992; Sikavitsas and Yang 1995). The irreversible thermodynamics approach considers the chemical potential gradient as the driving force for diffusion (Kärger and Bülow 1975; Kärger and Ruthven 1992). Multicomponent interactions occur through competitive equilibrium and/or diffusional sorbate–sorbate interactions. In this case, the driving force exerted on any particular species is balanced by the friction this species experiences with all other species present in the mixture and can be accurately described by the generalized Maxwell–Stefan (GMS) model for diffusion (Krishna 1987, 1990, 1993). Arguably, the Maxwell–Stefan formulation provides the most general, and the most convenient approach for describing mass transport which takes proper account of thermodynamic non-idealities and influence of external force fields. Furthermore, the Maxwell–Stefan approach can be extended to handle diffusion in macro- and micro-porous catalysts, adsorbents and membranes. Krishna and Wesselingh (1997) presented a comprehensive review on the application of the Maxwell–Stefan approach, as well as several examples illustrating the inadequacy of the Ficks's approach to modelling multi-component diffusion in micro-porous media. The applicability and advantages of the Maxwell–Stefan approach have been reviewed extensively by Van den Broeke and Krishna (1995), Krishna and Van den Broeke (1995), Bakker et al. (1997), Kapteijn et al. (2000), Krishna and Baur (2003), Krishna and van Baten (2005a, b, 2006), Krishna et al. (2004, 2007), Van de Graaf et al. (1999, 2000), Baker (2002), and Vareltzis et al. (2003).

Transport phenomena in porous solids have been the subject of many studies. Quantitative solutions are feasible only in few, relatively simple cases such as the permeation of a single gas. Separation of gas mixtures is much more complicated due to the complex membrane microstructure, large pressure gradients and extensive component interactions. In this work, a generic model of a porous membrane unit has been developed and consists of three coupled models:

- Permeate and retentate compartments (essentially the same transport phenomena)
- Micro-porous membrane
- Macro-porous support layer

The mass flux calculated in the membrane model is the link between the models: flux continuity equations must be satisfied at the interface between the retentate compartment and the membrane, between the membrane and the porous support, and between the porous support and the permeate compartment. The membrane unit topology is illustrated in Fig. 2.

Table 1 PSA governing equations

Bulk flow mass balance:

$$\varepsilon_{bed}\frac{\partial(uC_i)}{\partial z}+\varepsilon_{bed}\frac{\partial C_i}{\partial t}+(1-\varepsilon_{bed})N_i=\varepsilon_{bed}\frac{\partial}{\partial z}\left(D_{z,i}\frac{\partial C_i}{\partial z}\right),\forall z\in(0,\,L),\quad i=1,\ldots,N_{comp}$$

Concentration profile within the particle is assumed parabolic:

$$\frac{\partial\bar{Q}_i}{\partial t}=\frac{15D_{e,i}}{R_p^2}(Q_i^*-\bar{Q}_i),\quad \forall r\in[0,R_p],\ \forall z\in(0,\,L),\quad i=1,\ldots,N_{comp}$$

The generation term is sum of accumulation in gas phase in particles and amount adsorbed:

$$N_i=\rho^p\frac{\partial\bar{Q}_i}{\partial t}+\varepsilon_p\frac{\partial C_i}{\partial t},\quad \forall z\in(0,\,L),\quad i=1,\ldots,N_{comp}$$

Bulk flow heat balance:

$$\frac{\partial\left(\varepsilon_{bed}\rho c_p uT\right)}{\partial z}+\frac{\partial\left(\varepsilon_{bed}\rho c_p T\right)}{\partial t}+(1-\varepsilon_{bed})q_g+\frac{2k_{h,wall}}{R_{bed}}(T-T_{wall})=\varepsilon_{bed}\frac{\partial}{\partial z}\left(\lambda_z\frac{\partial T}{\partial z}\right),\forall z\in(0,\,L)$$

The generation term q_g is given by the sum of accumulations in gas and solid phase within the particles and heat of adsorption/desorption:

$$q_g=\frac{\partial[(\rho^p c_p^p+\varepsilon_p\rho_{pg}c_{p,pg})T]}{\partial t}\rho^p\sum_i^{N_{comp}}(\Delta H_{ads,i})\frac{\partial\bar{Q}_i}{\partial t},\quad \forall z\in(0,\,L)$$

Momentum balance (Blake–Kozeny equation):

$$-\frac{\partial P}{\partial z}=\frac{180\mu_{bg}u}{\left(2R_p\right)^2}\frac{(1-\varepsilon_{bed})^2}{\varepsilon_{bed}^3},\quad \forall z\in(0,\,L)$$

Boundary conditions for stream inlet into the bed:

$$u\left(C_i-C_i^{in}\right)=D_{z,i}\frac{\partial C_i}{\partial z},\quad z=0\text{ or }z=L,\quad i=1,\ldots,N_{comp}$$

$$T=T^{in},\quad z=0\text{ or }z=L$$

$$\frac{\partial u}{\partial z}=0,\quad z=0\text{ and }z=L$$

Boundary conditions for stream outlet from the bed or closed bed end:

$$\frac{\partial C_i}{\partial z}=0,\quad z=0\text{ or }z=L,\ i=1,\ldots,N_{comp}$$

$$\frac{\partial T}{\partial z}=0,\quad z=0\text{ or }z=L$$

$$\frac{\partial u}{\partial z}=0,\quad z=0\text{ and }z=L$$

Adsorption isotherm (Extended Langmuir):

$$Q_i^*=Q_{m,i}\frac{b_iC_i^p}{1+\sum_j b_jC_j^p},\quad \forall z\in[0,\,L],\ i,j=1,\ldots,N_{comp},\ b_i,Q_{m,i}=f(T,P)$$

Molecular diffusivity (Chapman–Enskog equation):

$$D_{m,i}=1.8583\times10^{-3}\sqrt{\frac{T^3\frac{1}{MW_i}}{P\sigma_{12}^2\Omega_{12}}},\quad \forall z\in[0,\,L],\ \forall r\in\left[0,\,R_p\right],\ i=1,2$$

Knudsen diffusivity (Kauzmann correlation):

$$D_{k,i}=9.7\times10^3R_{pore}\sqrt{\frac{T}{MW_i}},\quad \forall z\in[0,L],\ \forall r\in\left[0,\,R_p\right],\ i=1,\ldots,N_{comp}$$

Effective diffusivity:

$$D_{e,i}=\frac{\varepsilon_p}{\tau_p}\frac{D_{m,i}D_{k,i}}{D_{m,i}+D_{k,i}},\quad \forall z\in[0,\,L],\ \forall r\in\left[0,\,R_p\right],\ i=1,\ldots,N_{comp}$$

Gas valve equation: $F=C_v\,SP\,P_{in}\sqrt{A},\quad i=1,\ldots,N_{comp}$

if $P_{out}>P_{crit}\cdot P_{in}$: $\quad A=\left|\frac{1-(P_{out}/P_{in})^2}{\sum x_iMW_i\,T}\right|$

otherwise: $\quad A=\left|\frac{1-(P_{crit})^2}{\sum x_iMW_i\,T}\right|$

where critical pressure is: $\quad P_{crit}=\left(\frac{2}{1+\kappa}\right)^{\frac{\kappa}{1-\kappa}}$

Power for compression:

$$Power=\left(\tfrac{\kappa}{\kappa-1}\right)RT_{feed}\left(\left(\frac{P_{feed}}{P_{low}}\right)^{\frac{\kappa}{1-\kappa}}-1\right)\frac{N_{feed}}{\tau_{cycle}}$$

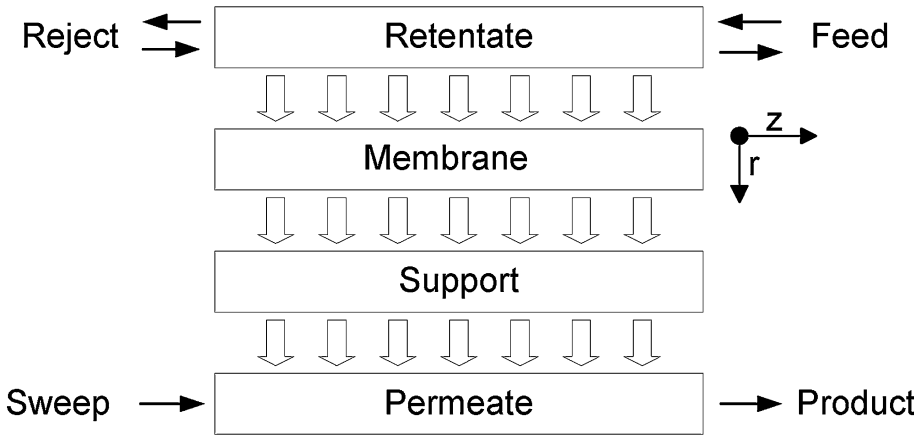

Fig. 2 The topology of the membrane unit

2.2.1 Permeate/retentate compartments

The main assumptions made in the model are:

- One dimensional flow pattern (axial domain)
- Ideal gas behavior
- Isothermal operation
- Negligible pressure drop
- The flow pattern is described by the axially dispersed plug flow

Mass balance for the axially dispersed plug flow is given by the following equation:

$$\frac{\partial(uC_i)}{\partial z} - D_{z,i}\frac{\partial^2 C_i}{\partial z^2} + a_V N_i = 0, \quad \forall z \in (0,L), \quad \forall i \in \{1,\ldots,N_{comp}\} \tag{1}$$

The generation term in Eq. (1) contains the molar flux N_i at each position along the compartment. The molar flux is calculated in the membrane model and coupled at the interfaces between the compartments and the membrane/support by the boundary conditions equations.

The boundary conditions at the inlet/outlet of the compartment depend on the operating mode of the module. Two operating modes have been developed:

- Co-current mode

$$u\left(C_i|_{z=0} - C_i^{in}\right) = D_{z,i}\frac{\partial C_i|_{z=0}}{\partial z}, \quad \forall i \in \{1,\ldots,N_{comp}\} \tag{2}$$

$$\left.\frac{\partial C_i}{\partial z}\right|_{z=L} = 0, \quad \forall i \in \{1,\ldots,N_{comp}\} \tag{3}$$

$$u|_{z=0} = u^{in} \tag{4}$$

$$\left.\frac{\partial u}{\partial z}\right|_{z=L} = 0 \tag{5}$$

- Counter-current mode

$$u\left(C_i|_{z=L} - C_i^{in}\right) = D_{z,i}\frac{\partial C_i|_{z=L}}{\partial z}, \quad \forall i \in \{1,\ldots,N_{comp}\} \tag{6}$$

$$\left.\frac{\partial C_i}{\partial z}\right|_{z=0} = 0, \quad \forall i \in \{1,\ldots,N_{comp}\} \tag{7}$$

$$u|_{z=L} = u^{in} \tag{8}$$

$$\left.\frac{\partial u}{\partial z}\right|_{z=0} = 0 \tag{9}$$

2.2.2 Porous membrane

The GMS equations provide an adequate basis for the description of multicomponent mass transfer in porous media as described by Krishna (1987, 1990, 1993). The Maxwell–Stefan approach is a convenient way to describe diffusion in porous media and yields coefficients that are directly amenable to physical interpretations. The GMS equations are based on the assumption that movement of species is caused by a driving force, which is balanced by the friction that the moving species experience from each other and their surroundings. Taking the gradient of the thermodynamic potential as the driving force and treating vacancies as participating species (representing zeolite) Krishna (1993) derived equations for the diffusion of adsorbed species.

Following the approach proposed by Krishna and Baur (2003) it is possible to independently combine the methods for computing the phase equilibria, the thermodynamic correction factor and the square matrix of inverse Maxwell–Stefan coefficients. A list of the implemented options is given below.

(a) Methods for calculating the phase equilibrium:

- Multicomponent Langmuir isotherm (single or dual site)

- Ideal Adsorbed Solution (IAS) theory
- Real Adsorbed Solution (RAS) theory

(b) Methods for the thermodynamic correction factor Γ:

- Unity matrix (no correction)
- Based on multicomponent Langmuir isotherm (single or dual site)
- Based on IAS theory
- Based on RAS theory

(c) Methods for the square matrix of inverse Maxwell–Stefan coefficients $\mathcal{D}_{ij}$:

- No binary diffusional interactions
- Binary interaction estimated from the Vignes equation

The membrane is connected at one side to a retentate compartment and to a support layer at the other and the boundary conditions at each of two interfaces ensure the mass flux continuity between them.

The main assumptions made in the model are:

- Two dimensional flow pattern (axial and radial domain)
- Ideal gas behaviour
- Isothermal and the steady state operation
- All adsorption happens at the membrane interfaces ($r = 0$ and $r = \delta_m$)
- At the steady state, gas is in equilibrium with the membrane surface
- Inside the membrane gas is transported by surface diffusion
- The flux is constant along the membrane (r axis direction)

Three options are available to describe multi-component diffusion in micro-porous media (adsorbate phase):

- Assuming that the Fick law applies (useful during the initialization of the DAE system):

$$N_i = -\frac{\rho q_i^{sat} \mathcal{D}_i^s}{RT}\frac{\partial \theta_i}{\partial r},\ z \in [0,L],\ r \in [0,\delta_m),\quad \forall i \in \{1,\ldots,N_{comp}\} \tag{10}$$

- Assuming friction between molecules less important than friction with the wall; in that case $\mathcal{D}_{ij}^s$ is much larger than $\mathcal{D}_i^s$ and this case is referred to as the "single-file" diffusion mode and given by the following equation:

$$N_i = -\frac{\rho q_i^{sat} \mathcal{D}_i^s}{RT}\sum_{j=1}^{N_{comp}} \Gamma_{ij}\frac{\partial \theta_i}{\partial r},\ z \in [0,L],\ r \in [0,\delta_m),\quad \forall i,j \in \{1,\ldots,N_{comp}\} \tag{11}$$

- If sorbate–sorbate interactions cannot be neglected, the general Maxwell–Stefan equations are used:

$$\frac{\theta_i}{RT}\frac{\partial \mu_i}{\partial r} = \sum_{\substack{j=1\\ j\neq i}}^{N_{comp}} \frac{q_j N_i - q_i N_j}{q_i^{sat} q_j^{sat} \mathcal{D}_{ij}^s} + \frac{N_i}{q_i^{sat}\mathcal{D}_i^s},\quad z \in [0,L],\ r \in [0,\delta_m),\quad \forall i,j \in \{1,\ldots,N_{comp}\} \tag{12}$$

For calculation of the cross-term diffusivities ($\mathcal{D}_{ij}^s$) Krishna (1993) proposed to use the empirical relation of Vignes to determine $\mathcal{D}_{ij}^s$ from the single-component diffusivities:

$$\mathcal{D}_{ij}^s = \left(\mathcal{D}_i^s\right)^{\frac{\theta_i}{\theta_i+\theta_j}}\left(\mathcal{D}_j^s\right)^{\frac{\theta_j}{\theta_i+\theta_j}},\ z \in [0,L],\ r \in [0,\delta_m),\quad \forall i,j \in \{1,\ldots,N_{comp}\} \tag{13}$$

The gradient of the surface chemical potential $\frac{\partial \mu_i}{\partial r}$ in Eq. (12) may be expressed in terms of the gradients of the surface occupancies by introduction of the thermodynamic factor Γ:

$$\frac{\theta_i}{RT}\frac{\partial \mu_i}{\partial r} = \sum_{j=1}^{N_{comp}} \Gamma_{ij}\frac{\partial \theta_i}{\partial r},\quad z \in [0,L], r \in [0,\delta_m],\quad \forall i,j \in \{1,\ldots,N_{comp}\} \tag{14}$$

where the thermodynamic factor Γ is given by:

$$\Gamma_{ij} = \theta_i \frac{\partial \ln p_i}{\partial \theta_j} = \frac{q_j^{sat}}{q_i^{sat}}\frac{q_i}{p_i}\frac{\partial p_i}{\partial q_j} = \frac{\theta_i}{p_i}\frac{\partial p_i}{\partial \theta_j},\quad z \in [0,L], r \in [0,\delta_m], \forall i,j \in \{1,\ldots,N_{comp}\} \tag{15}$$

In general, the partial derivative $\frac{\partial p_i}{\partial \theta_j}$ depends on the adsorption isotherm employed as follows:

$$\frac{\partial p_i}{\partial \theta_j} = \frac{\partial p_i(T,P,\theta,adsorption\ isotherm)}{\partial \theta_j} \tag{16}$$

In the case that the Extended Langmuir adsorption isotherm is used, the partial derivative $\frac{\partial p_i}{\partial \theta_j}$ can be derived from the isotherm equation and given in an explicit form as follows (Krishna 1993):

$$\Gamma_{ij} = \frac{\theta_i}{p_i}\frac{\partial p_i}{\partial \theta_j} = \begin{cases} 1 + \dfrac{\theta_i}{1-\sum_k \theta_k}, & i = j \\ \dfrac{\theta_i}{1-\sum_k \theta_k}, & i \neq j \end{cases},\quad \forall z \in [0,L],\quad \forall i,j,k \in \{1,\ldots,N_{comp}\} \tag{17}$$

If the IAS or RAS are used, the partial derivative $\frac{\partial p_i}{\partial \theta_j}$ cannot be given in an explicit form and has to be calculated numerically (Krishna and Paschek 2000).

At the steady state, gas is in equilibrium with the membrane surface, given by:

$$\theta_i|_{r=0} = \frac{q_i^*(T,P,x)\big|_{r=0}}{q_i^{sat}} = f(P,T,x), \quad \forall z \in [0,\, L], \quad \forall i \in \{1,\ldots,N_{comp}\} \tag{18}$$

$$\theta_i|_{r=\delta m} = \frac{q_i^*(T,P,x)\big|_{r=\delta m}}{q_i^{sat}} = f(P,T,x), \quad \forall z \in [0,\, L], \forall i \in \{1,\ldots,N_{comp}\} \tag{19}$$

2.2.3 Support layer

In most cases *the resistance of the support* layer cannot be neglected. Although diffusion in the support is relatively fast compared to diffusion in the zeolite layer, the support thickness and low porosity causes significant partial-pressure gradients that influence the boundary condition at the membrane-support interface (Van de Graaf et al. 1999).

The general Maxwell–Stefan equations can be used to calculate the partial-pressure gradient in the support layer, now applied to gas-phase diffusion (Krishna 1993). According to Krishna, three fundamentally different diffusion mechanisms exist inside the pores of the porous media:

- Bulk (free molecular) diffusion where molecule–molecule collisions dominate over molecule–wall collisions; it becomes significant for large pore sizes and high system pressures
- Knudsen diffusion where molecule–wall collisions dominate; it is predominant when the mean free path of the molecular species is much larger than the pore diameter
- Surface diffusion of adsorbed molecular species along the pore surface; it is predominant for micro-pores and for strongly adsorbed species

For a macroporous support, the free molecular diffusion is predominant and the contribution of the other two mechanisms is very low because the pores are large and the support is inert. The support layer is connected at two sides to the membrane and the permeate compartment and the boundary conditions at each of two interfaces ensure mass flux continuity between them.

The main assumptions made in the model are:

- Two dimensional flow pattern (axial and radial domain)
- Ideal gas behaviour
- Isothermal and the steady state operation
- The support layer is inert and macroporous
- Gas is transported by molecular diffusion (pores and/or pressure is large enough so that Knudsen diffusion is negligible)
- The flux is constant along support layer and equal to the flux through the membrane

To describe multi-component diffusion in the gas phase of the macro-porous media two options are available:

(a) Assuming that the Fick law holds,

$$N_i = -\frac{\varepsilon \mathcal{D}_{ij}}{RT}\frac{\partial p_i}{\partial r},\ z \in [0,L],\ r \in (0,\delta_s], \quad \forall i \in \{1,\ldots,N_{comp}\} \tag{20}$$

(b) If molecule–molecule interactions cannot be neglected, the GMS equations (with no Knudsen diffusivity term) are used (Krishna 1993):

$$-\frac{1}{RT}\frac{\partial p_i}{\partial r} = \sum_{j=1}^{N_{comp}} \frac{x_j N_i - x_i N_j}{\varepsilon \mathcal{D}_{ij}},\ z \in [0,L],\ r \in (0,\delta_s], \quad \forall i,j \in \{1,\ldots,N_{comp}\} \tag{21}$$

If sweep gas is used, Eq. (21) is given in the following form:

$$-\frac{1}{RT}\frac{\partial p_i}{\partial r} = \sum_{j=1}^{N_{comp}} \frac{x_j N_i - x_i N_j}{\varepsilon \mathcal{D}_{ij}} + \frac{x_{inert} N_i - x_i N_{inert}}{\varepsilon \mathcal{D}_{i,inert}}, \quad z \in [0,L], r \in (0,\delta_s], \quad \forall i,j \in \{1,\ldots,N_{comp}\} \tag{22}$$

where $N_{inert} = 0$, $x_{inert} = 1 - \sum_{NoComp} x_j$ and $\mathcal{D}_{i,inert} = \mathcal{D}_i$

Finally, the GMS equations in the case when sweep gas is used become:

$$-\frac{1}{RT}\frac{\partial p_i}{\partial r} = \sum_{j=1}^{N_{comp}} \frac{x_j N_i - x_i N_j}{\varepsilon \mathcal{D}_{ij}} + \frac{\left(1 - \sum_{k=1}^{NoComp} x_k\right) N_i}{\varepsilon \mathcal{D}_i}, \quad z \in [0,L],\ r \in (0,\delta_s], \quad \forall i,j,k \in \{1,\ldots,N_{comp}\} \tag{23}$$

2.3 Hybrid PSA/membrane

All previously described models are developed to be compatible with the gPROMS PML standard library. The PSA and membrane models can then be easily coupled. Thus, hybrid schemes can simply be developed by dragging and dropping those models into the flowsheet without an additional modelling required.

3 Definition of the optimization problem

The hybrid PSA/membrane modelling and optimization framework has been applied to the process of hydrogen recovery from SMROG. Hybrid PSA/Membrane separation units offer some (ideally all) of the following advantages:

- Increase in product purity.
- Increase in product recovery.
- Increase in the productivity of the adsorbent (i.e. process more feed by the same amount of adsorbents, or the same amount of feed by the lower amount of adsorbents).
- Decrease in capital cost (by decreasing the beds size or number of beds).
- Removal of some common pollutants (CO and CO_2).
- Fractionation of some valuable components from the mixture, which are usually wasted.

The PSA technology is already capable of producing hydrogen of very high purity (99.999+ %) and further improvements are neither easy nor commonly required. Thus, the focus in this work is to achieve the other objectives: to increase hydrogen recovery, increase adsorbent productivity (i.e. decrease the size of beds), decrease capital costs, and capture the carbon monoxide and carbon dioxide in a secondary stream.

In order to systematically investigate the coupling of PSA and membrane units two base schemes have been recognized:

(I) PSA serves as the main bulk separation unit
(II) Membrane serves as the main bulk separation unit

Base scheme I assumes that membrane is an aid to a PSA module providing the following functionality:

(a) Membrane(s) attached to feed stream (pressurization and adsorption steps):
   - to decrease the concentration of impurities

(b) Membrane(s) attached to waste gases streams (blowdown and purge steps):
   - to recover product (H_2)
   - to remove certain impurities (such as CO or CO_2)
   - to fractionate the gas mixture by producing secondary product

(c) Membranes(s) attached to both feed and waste gases streams:
   - all of the abovementioned

(d) Membrane(s) attached to product stream (adsorption step):
   - to purify crude product from PSA unit

Base scheme II assumes that PSA is an aid to membrane module providing the following functionality:

(a) PSA attached to permeate stream:
   - to recover product (H_2)
   - to remove certain impurities (such as CO or CO_2)

(b) PSA attached to retentate stream:
   - to purify crude product mixture from membrane

In the work of Esteves and Mota (2007) the hybrid concept exploited the base scheme II and was formulated to address both cooperative and opposing regions of the selectivity for the two stand-alone units, and two main schemes were developed:

- Scheme A, in which the more permeable component is the least adsorbed one
- Scheme B, in which the more permeable component is the more adsorbed one

In this work, we focus on base scheme I which can be exploited in many different ways. In a general case, we have several streams entering or leaving a bed:

- At the top of the bed: product, depressurization, purge and pressurization (by pure light product) streams
- At the bottom of the bed: feed, pressurization (by feed), blowdown and purge streams

All streams are shown in Fig. 3. There are no benefits to attach a membrane on a product stream as purity is already sufficiently high. A depressurization stream of high-enough purity is used to pressurize or purge other beds as well. The same stands for all streams at the top of the bed. However, all streams at the bottom of the bed can be pre- or post-processed by using one or several membrane units. Feed and pressurization streams can be processed in order to decrease the level of impurities in feed that are allowed to enter the bed and to capture a secondary stream of CO and CO_2. On the other hand, the waste gases that leave the bed during blowdown and purge steps can be processed in order to either increase the recovery of the light product, recover some valuable components (H_2 and CH_4) and to decrease the level of pollutants (CO and CO_2).

Therefore, three different configurations have been recognized by the present analysis as feasible:

- A membrane attached to the feed stream (adsorption): *Mem-PSA*
- A membrane attached to the waste gases streams (blowdown and purge): *PSA-Mem*
- Membranes attached to both feed and waste gases streams: *Mem-PSA-Mem*

The objective in the present work is to analyze these three hybrid configurations and to compare their separation performance to the base *PSA-Only* case. In order to make a fair comparison among the various configurations involving PSA, it is first necessary to make certain assumptions. The total cycle time, the amount of feed and the bed diameter are kept constant (to make comparison of beds easier). Based on the conclusions from our previous work

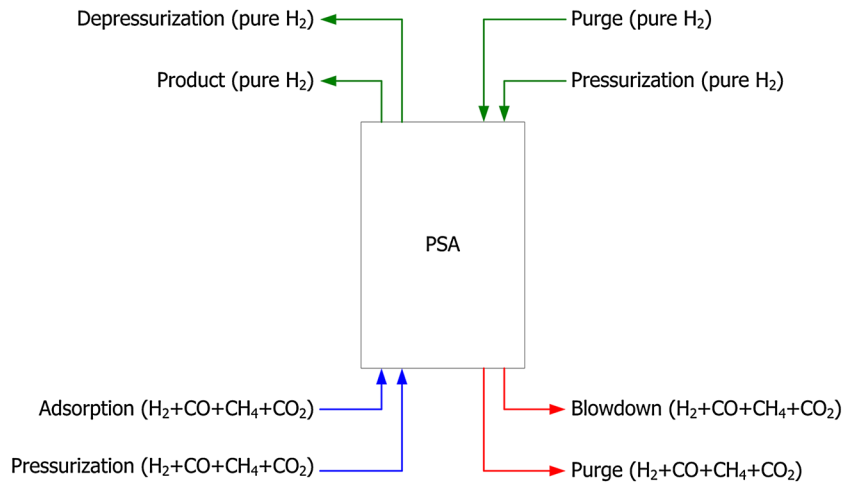

Fig. 3 Basic inlet/outlet streams in a PSA unit

(Nikolic et al. 2009), the most significant process parameters in this separation process are the feed pressure, bed geometry (length-to-diameter ratio), purge-to-feed ratio and carbon-to-zeolite ratio (for two-layered beds).

The next issue addressed is the type of membrane that should be employed. Since the objective in this work is to use a PSA as the main separation unit, the logical choice is to use a CO_2 selective membrane to decrease the level of impurities that enter the bed and to capture CO and CO_2 in a separate stream. For instance, using a hydrogen selective membrane, PSA is transformed into the auxiliary unit. For processing of the waste gases a CO_2 selective membrane should be used again. The objective here is to capture CO and CO_2 in a separate stream.

3.1 Base case (*PSA-Only*)

The optimization problem is formulated as the maximization of hydrogen recovery for given minimum requirements in hydrogen purity, while optimizing the number of beds and cycle configuration, feed pressure, purge-to-feed ratio, carbon-to-zeolite ratio, and bed length (cycle and step times, the amount of feed and bed diameter were kept constant):

$$
\begin{aligned}
Max \quad & Recovery_{H_2} \\
s.t. \quad & Model\ Equations \\
& Purity_{H_2} \geq 99.99\,\% \\
& N_{beds} \in \{1, 2, 4, 5, 8\} \\
& Configurations \in \{C1, C2, C4, C5a, C5b, C8\} \\
& LB \leq P_{feed} \leq UB \\
& LB \leq \frac{Purge}{Feed} ratio \leq UB \\
& LB \leq L \leq UB \\
& LB \leq \frac{Carbon}{Zeolite} ratio \leq UB \\
& LB \leq \frac{Carbon}{Zeolite} ratio \leq UB
\end{aligned}
\tag{24}
$$

where LB and UB denote the lower and upper bounds of optimization variables, respectively.

3.2 Case 1: Membrane attached to the feed stream (*Mem-PSA*)

This hybrid separation scheme consists of a membrane and a PSA unit which is connected to a retentate stream of the CO_2 selective membrane (Fig. 4). The role of the membrane is to remove impurities from the feed stream sent to the PSA (retentate stream) and to capture CO and CO_2 in a secondary stream (permeate stream). The goal is to maximize the hydrogen recovery while controlling the carbon dioxide concentration in the membrane retentate that enters the PSA unit. Therefore, several changes have to be introduced to the problem definition compared to the *PSA-Only* case. First, the objective function in this case must be the maximization of the overall hydrogen recovery, a combined recovery of the membrane and the PSA unit. Second, three new design optimization variables were added to the optimization problem: membrane area, thickness and support thickness. Permeate side pressure and temperature were kept constant. Finally, two issues became obvious from the preliminary optimization runs:

- If a feed pressure is considered common for PSA and membrane, much lower hydrogen recovery can be obtained compared to *PSA-Only* case. Thus, it is desirable to allow PSA and membrane feed pressures to be different, by introducing an additional constraint that the PSA feed pressure must be lower or equal to the membrane feed pressure. This approach produced satisfactory results
- To study the effect of the carbon dioxide content in the PSA feed stream, a new constraint was introduced representing the maximum concentration of the carbon dioxide in the membrane retentate stream

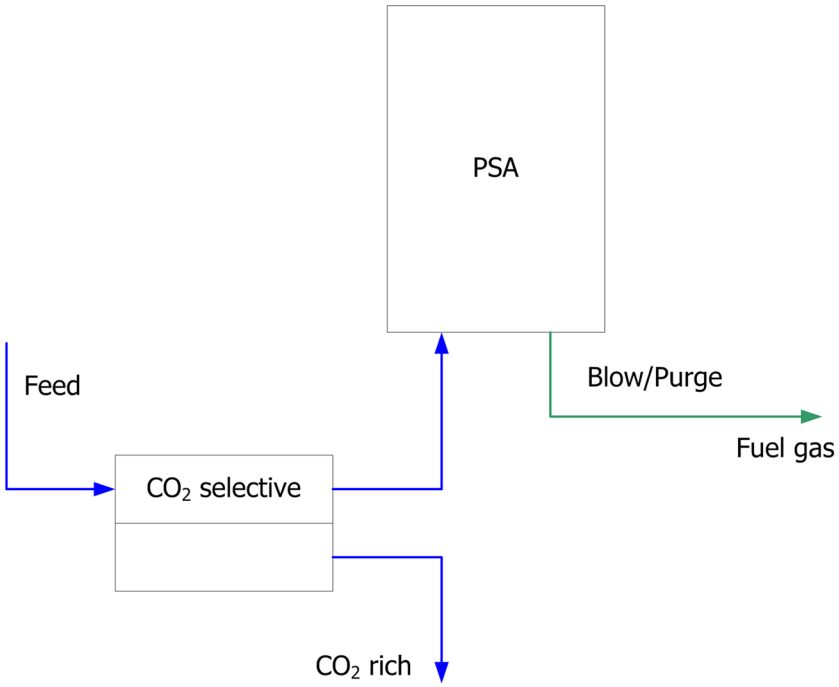

Fig. 4 Schematic flowchart for hybrid scheme 1: *Mem-PSA*

Keeping the above notes in mind, the optimization problem is now formulated as the maximization of overall hydrogen recovery for given minimum requirements in hydrogen purity and maximum allowed carbon dioxide concentration in the membrane retentate stream, an input for PSA, while optimizing the number of beds and cycle configuration, PSA feed pressure, purge-to-feed ratio, carbon-to-zeolite ratio, bed length, membrane feed pressure, membrane area, and membrane and the support thickness. Cycle and step times, the amount of feed, bed diameter, permeate side pressure and temperature were kept constant, with an additional constraint on the membrane and the PSA feed pressures:

$$
\begin{aligned}
Max \quad & Overall Recovery_{H_2} \\
s.t. \quad & Model\ Equations \\
& Purity_{H_2} \geq 99.99\,\% \\
& N_{beds} \in \{1, 2, 4, 5, 8\} \\
& Configurations \in \{C1, C2, C4, C5a, C5b, C8\} \\
& LB \leq P_{feed}^{PSA} \leq UB \\
& LB \leq \frac{Purge}{Feed} ratio \leq UB \\
& LB \leq L \leq UB \\
& LB \leq \frac{Carbon}{Zeolite} ratio \leq UB \\
& LB \leq A_{membrane} \leq UB \\
& LB \leq \delta_{membrane} \leq UB \\
& LB \leq \delta_{support} \leq UB \\
& LB \leq P_{feed}^{Membrane} \leq UB \\
& P_{feed}^{PSA} \leq P_{feed}^{Membrane} \\
& x_{CO_2} \in \{3, 4, 5 \text{ and } 6\,\%\}
\end{aligned}
\tag{25}
$$

where LB and UB denote the lower and upper bounds of optimization variables, respectively.

In our case four different cases have been investigated where CO_2 concentration coming out of the membrane was fixed to 3–6 % (the CO_2 concentration in the feed is 17 %). This way, Pareto curves can be constructed with the overall recovery given as a function of CO_2 concentration after the membrane unit and trade-offs between hydrogen recovery and carbon dioxide content investigated. The outlet CO_2 concentrations were limited to the 3–6 % range because in the cases with less than 3 % of CO_2 too much H_2 is lost through the membrane leading to a poor overall recovery, while in the cases with more than 6 % too little CO_2 is removed and the benefits of the hybrid schemes are lost.

3.3 Case 2: Membrane attached to the waste gases stream (*PSA-Mem*)

This hybrid separation scheme consists of a PSA and a CO_2 selective membrane unit which is connected to the waste gases stream from the PSA during the blowdown and purge steps (Fig. 5). PSA and the membrane unit are connected via a compressor since the waste gases are available at low pressures. The role of the membrane is to capture CO and CO_2 in a secondary stream (permeate stream). It follows

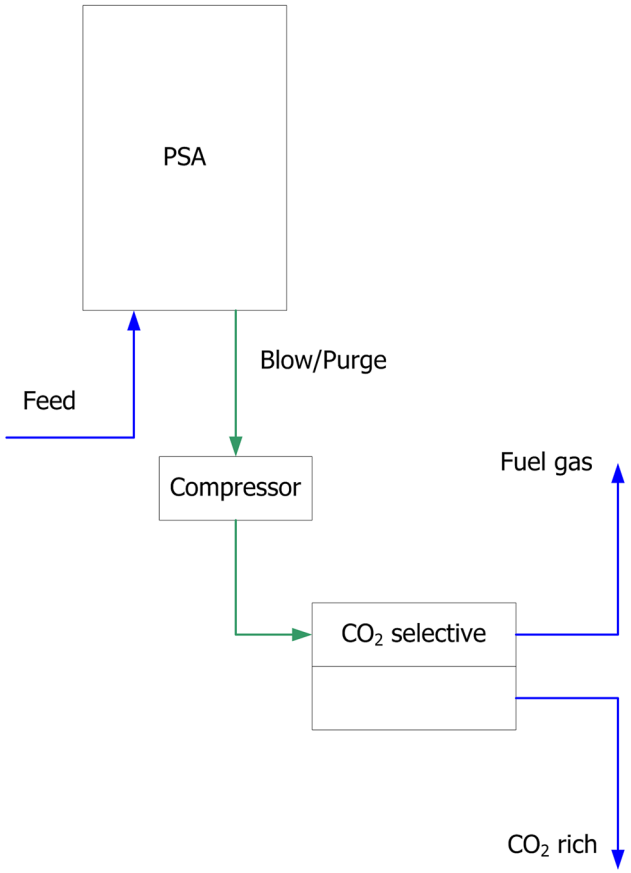

Fig. 5 Schematic flowchart for hybrid scheme 2: *PSA-Mem*

that we now have two targets: (a) to maximize hydrogen recovery; (b) to maximize H_2 and CH_4 concentrations in the membrane retentate stream. These two objectives are not interdependent, since the primary objective is to maximize hydrogen recovery, and the optimization problem can be split into two smaller problems. First, the PSA unit is optimized; then, starting with the waste gases from the PSA unit with combined blowdown and purge off gases and using an average composition, flowrate and temperature, the optimization problem is solved for the second objective. Obviously, the first objective is identical to the *PSA-Only* case. Consequently, the optimization results of the first problem should be equal to the results from the *PSA-Only* case (which is actually the case, as it will be shown in the section with the results). The mathematical formulation of the PSA optimization problem is given previously by Eq. (24). The membrane optimization problem can be formulated as the maximization of the combined H_2 and CH_4 concentration in the membrane retentate stream of the membrane system downstream the PSA, while optimizing the membrane feed pressure (since the waste gases are available at low pressures), membrane area, and membrane and support thickness (permeate side pressure is kept constant, while the temperature is equal to the average temperature of waste gases):

$$\begin{aligned} Max \quad & (x_{H_2} + x_{CH_4}) in\ retentate \\ s.t. \quad & Model\ Equations \\ & LB \le P_{feed} \le UB \\ & LB \le A_{membrane} \le UB \\ & LB \le \delta_{membrane} \le UB \\ & LB \le \delta_{support} \le UB \end{aligned} \tag{26}$$

3.4 Case 3: Membranes attached to both feed and waste gases streams (*Mem-PSA-Mem*)

This hybrid separation scheme consists of the *Mem-PSA* scheme (membrane + PSA) with an additional CO_2 selective membrane unit connected to the waste gases stream from the PSA during the blowdown and purge steps (Fig. 6). PSA and the second membrane unit are connected via a compressor. Again, we have two objectives: a) to maximize hydrogen recovery; b) to maximize H_2 and CH_4 concentrations in the membrane retentate stream. In this scheme we have two CO + CO_2 secondary streams (permeate streams from both membranes). All the conclusions made for the *PSA-Mem* case hold here as well: we have two objectives and we can split the optimization problem into two smaller problems. In this case, the PSA and the first membrane unit will be optimized together; then, starting with the waste gases from the *Mem-PSA* case (combined blowdown and purge off gases) of the average composition, flowrate and temperature the second problem is solved. Once more, the optimization results of the first problem should be equal to the results from the *Mem-PSA* case. The mathematical formulation of the *Mem-PSA* optimization problem is given by Eq. (25), while the mathematical formulation of the membrane attached to the waste gas stream is given by Eq. (26).

4 Optimization results and discussion

The input to all four optimization cases is the SMROG of the same characteristics, given in Table 2. For all four cases, configurations *C1*, *C2*, *C4*, *C5a*, *C5b* and *C8* have been employed as described in Nikolic et al. (2009) and two adsorbent layers have been used (activated carbon and zeolite 5A). In practice, the configuration C8 requires a variable overall feed and purge flow-rates to work in an actual experiment. Nevertheless, it is used in the present study to compare a configuration with three pressure equalization steps to more efficient configurations C4 and C5b that employ an additional co-current depressurization step after the pressure equalizations. All transport and

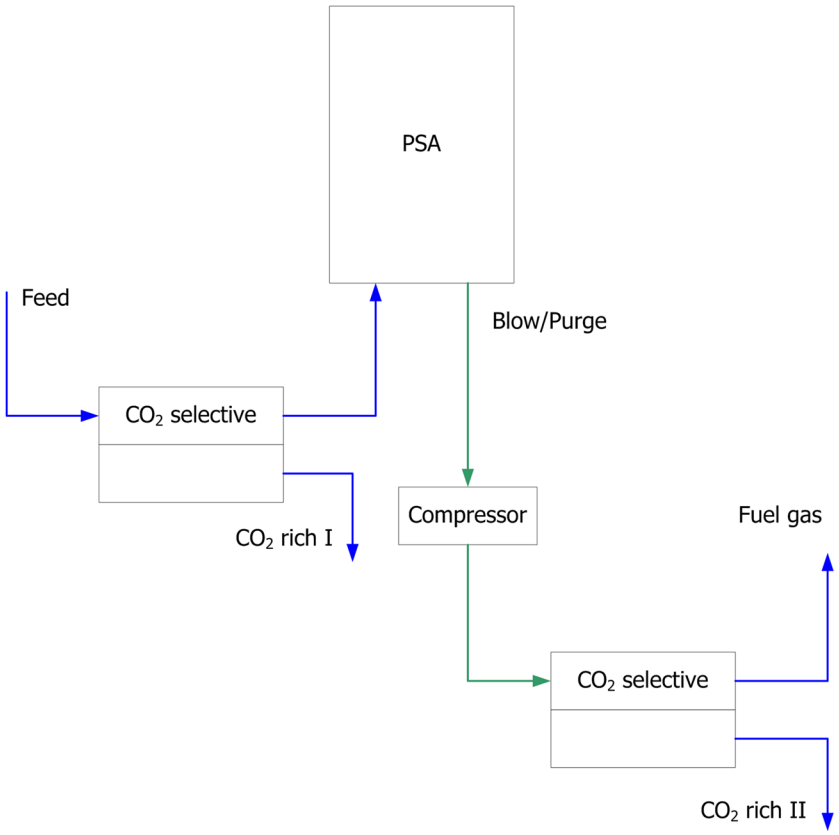

Fig. 6 Schematic flowchart for hybrid scheme 3: *Mem-PSA-Mem*

equilibrium properties for PSA are equivalent to those in Nikolic et al. (2009). Silicalite-1 membrane with a stainless steel support layer has been selected. Silicalite-1 has been chosen because it is CO_2 selective and extensively, both theoretically and experimentally, investigated in the literature. Adsorption isotherm data and surface diffusion coefficients for Silicalite-1 membrane are adopted from the work of Bakker et al. (1997). Base case parameters for adsorption bed and membrane are also given in Table 2, while PSA runtime parameters are given in Table 3. Molecular diffusivities through the metal support are calculated using Chapman–Enskog's equation.

Upper and lower bounds of the optimization variables were as follows:

- Purge-to-feed ratio (0.5–2.5)
- Feed pressure (5–30 bar)
- Carbon-to-zeolite ratio (0.25–0.75)
- Length-to-diameter ratio (hybrid configurations: 5–15, PSA-Only: 5–20)
- Membrane area (0.1–5 m^2)
- Membrane thickness (0.1×10^{-5}–5×10^{-5} m)
- Support thickness (1–10 mm)

All optimization problems have been solved using the Process Systems Enterprise (2011) gPROMS/gOPT modelling and optimization software. The axial domains for each layer have been discretized using Orthogonal Collocation on Finite Elements (OCFEM) of third order. 20 elements per layer have been used giving a total of 40 elements per bed. Axial domains in the retentate and permeate compartments have been discretized using OCFEM of third order and 20 elements. Radial domain in the membrane model has been discretized using OCFEM of third order and 4 elements as no steep profiles were observed along that direction.

The computational time depends on the complexity of the particular optimization problem. The typical wall-time required for the computations of the Mem-PSA case on AMD Phenom II X4 810 running on 2.6 GHz ranged from 14 and up to 60 h CPU time, depending on the PSA configuration complexity. These values are significantly higher compared to the PSA only case. More particularly the CPU time required to run the optimization problem in C1 configuration increases from 5 h for the PSA only case to 14 h for the Mem-PSA case. For the C8 configuration the respective values are 20 h for the PSA only case and 60 h for the Mem-PSA case. For the PSA-Mem case, where membrane optimization is uncoupled from PSA the required CPU time for former was minimal in all runs (3–6 min). The same holds for the Mem-PSA-mem case, where the optimization of the second membrane is uncoupled with the Mem-PSA unit, so each of the two was optimized separately.

Table 2 Base case feed characteristics and input parameters for adsorption column and membrane

Parameter	Value			
	H_2	CO	CH_4	CO_2
Composition (%)	75.5	4.0	3.5	17.0
Flowrate (lit_{STP}/s)	2.5			
Temperature (K)	303			

	Value
Adsorption column characteristics	
Length (m)	1.0
Diameter (m)	0.1
AC/zeolite ratio	1
Membrane characteristics	
Membrane surface (m^2)	0.5
Membrane thickness (m)	1×10^{-5}
Support thickness (m)	3×10^{-3}
Feed pressure (bar)	10
Permeate pressure (Pa)	1×10^{5}

Table 3 PSA runtime parameters (all case studies)

Parameter	Configuration					
	C1	C2	C4	C5a	C5b	C8
$\tau_{PressCC\ (s)}$	120	60	60	48	48	60
$\tau_{Ads\ (s)}$	120	120	120	96	96	90
$\tau_{PEQ1\ (s)}$	–	60	60	48	48	30
$\tau_{PEQ2\ (s)}$	–	–	–	48	48	30
$\tau_{PEQ3\ (s)}$	–	–	–	–	–	30
$\tau_{CoCD\ (s)}$	–	–	60	–	48	–
$\tau_{Purge\ (s)}$	120	60	60	48	48	60
$\tau_{Blow\ (s)}$	120	120	60	96	48	90
$\tau_{cycle\ (s)}$	480	480	480	480	480	480

The overall conclusion from the optimization results is that by using hybrid schemes it is possible to increase the hydrogen recovery ($\sim$2 %), significantly decrease the size of beds (up to 46 %) and hence increase adsorbent productivity up to 184 %, capture the carbon monoxide and carbon dioxide in a secondary stream (up to 76 % of carbon monoxide and carbon dioxide combined), and significantly (up to 74 %) reduce carbon dioxide concentration in PSA waste gases. It should be noted that the carbon dioxide rich stream produced by the membrane is of moderate purity, not suitable for immediate sequestration and has to be further processed or a different type of membrane be used.

In this work, an increase in adsorbent productivity is achieved by decreasing the size of beds by decreasing the amount of adsorbent. This way the same amount of feed can be processed by a lower amount of adsorbent. However, an increase in adsorbent productivity is also registered by leaving the bed size intact so that more feed can be processed by the same amount of adsorbent due to the lower concentration of impurities. The later may be a preferred option in the case of the existing PSA plant.

4.1 Base case and case 1: *PSA-Only* and *Mem-PSA*

4.1.1 Recovery

Comparison of the overall H_2 recovery in *Mem-PSA* and H_2 recovery in *PSA-Only* case, for all PSA configurations and different CO_2 concentrations in the membrane retentate, is presented in Fig. 7. We can observe that the overall H_2 recovery in the *Mem-PSA* case is higher, up to 2 %, compared to the *PSA-Only* case, except for C1 and C5a configurations. Also, there is a trade-off between H_2 recovery and CO_2 concentration in the membrane retentate, used as a feed input stream for PSA beds. As the CO_2 content increases, for all configurations, recovery increases as well. This effect is more pronounced in configurations C1, C4 and C8.

The highest recovery is produced by the configurations C4 and C5b. They differ from the others in that they operate an additional co-current depressurization step (after the pressure equalization steps) where the produced gas is used to purge other columns. The combination of pressure equalization and co-current depressurization steps leads to a much higher recovery compared to the configurations with the pressure equalization only. The reason is that the pressure equalizations re-use a good portion of the void gases but not completely, since the end pressure is always higher than the purge gas pressure. If an additional co-current depressurization step is used the whole amount of void gases can be conserved, subject to certain limitations: the column can be depressurized only up to the point where the strongly adsorbed species start to breakthrough, otherwise the other column undergoing purge step would be contaminated with the strongly adsorbed species.

4.1.2 Length-to-diameter ratio

Comparison of the length-to-diameter ratio in *Mem-PSA* and length-to-diameter ratio in *PSA-Only* case, for all configurations and different CO_2 content in the membrane retentate, is presented in Fig. 8. Since the bed diameter has been kept constant in all studies these results directly represent the difference in size of the beds or in the other words a difference in the amount of the adsorbent. It can be observed that length-to-diameter ratio in *Mem-PSA* cases follows a similar trend, but it is always lower compared to *PSA-Only* case, which can be attributed to a much higher

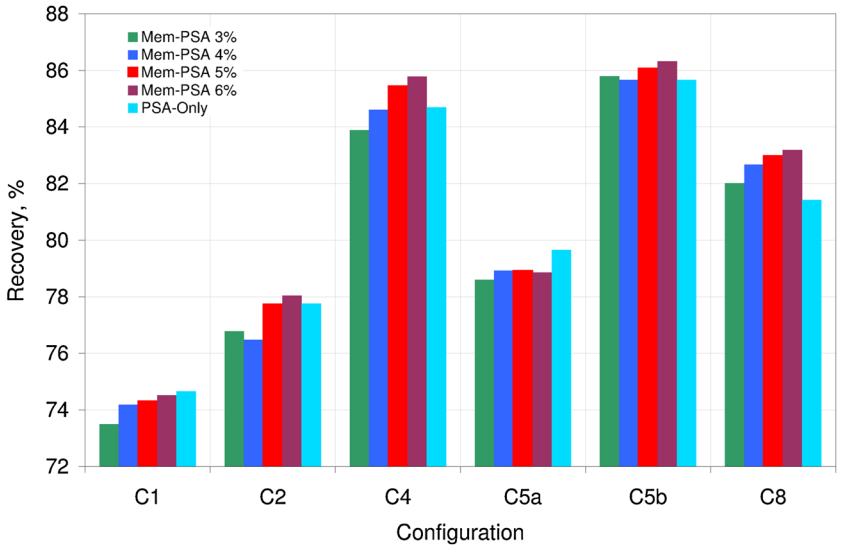

Fig. 7 Comparison of the overall maximum H_2 recovery in *Mem-PSA* to H_2 recovery in *PSA-Only* case (for all configurations and different CO_2 contents in the membrane retentate stream)

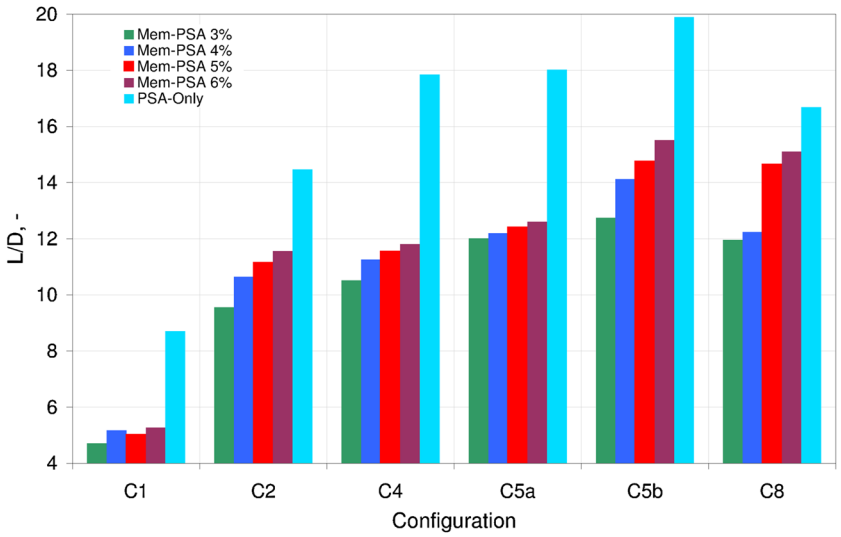

Fig. 8 Comparison of the optimal values of length-to-diameter ratio in *Mem-PSA* to those obtained in *PSA-Only* case (for all configurations and different CO_2 contents in the membrane retentate stream)

CO_2 content in feed in *PSA-Only* case; consequently, longer beds are needed to achieve the same purity. Also, as the CO_2 content in feed stream increases—the length-to-diameter ratio increases as well for all but one configuration: C1–4 % CO_2, which can be attributed to numerical issues. This is an expected result when the amount of impurities increases, longer beds are needed to achieve the same purity.

It can be concluded that it is possible to achieve a reduction in bed size, in amount of an adsorbent, up to 46 % for the case of 3 % CO_2. In conclusion, the capital cost and the adsorbent productivity can be significantly improved by using this hybrid scheme.

4.1.3 Carbon-to-zeolite ratio

Comparison of the carbon-to-zeolite ratio in *Mem-PSA* to the carbon-to-zeolite ratio in *PSA-Only* case, for all configurations and different CO_2 contents in the membrane retentate is given in Fig. 9. It can be seen that the carbon-to-zeolite ratio is lower compared to *PSA-Only* case, for most configurations. This trend is expected since the CO_2 content is lower, thus, the activated carbon layer can be shorter. Furthermore, it can be noted that as the CO_2 content increases the carbon-to-zeolite ratio increases too, for all configurations because of a higher amount of CO_2 in the feed stream. Thus, the activated carbon layer must be longer to produce H_2 of the same purity.

4.1.4 Purge-to-feed ratio

Comparison of the optimal purge-to-feed ratio in *Mem-PSA* to the purge-to-feed ratio in *PSA-Only* case for all configurations and different CO_2 contents in the membrane retentate is presented in Fig. 10. It is seen that the optimal purge-to-feed ratio follows the same trend and it is always

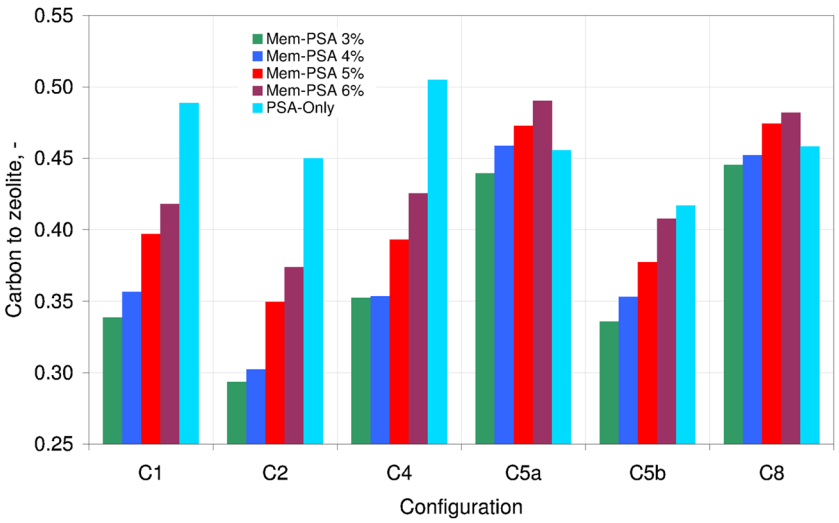

Fig. 9 Comparison of the optimal values of carbon-to-zeolite ratio in *Mem-PSA* to those obtained in *PSA-Only* case (for all configurations and different CO_2 contents in the membrane retentate stream)

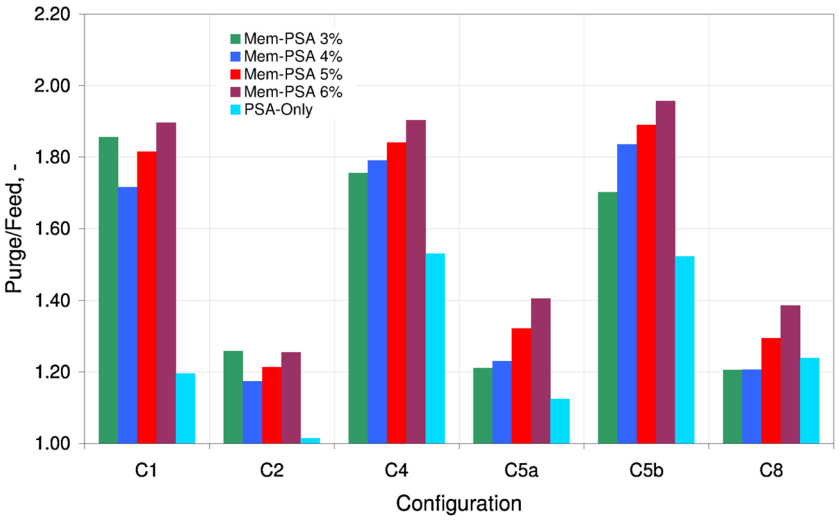

Fig. 10 Comparison of the optimal values of purge-to-feed ratio in *Mem-PSA* to those obtained in *PSA-Only* case (for all configurations and different CO_2 contents in the membrane retentate stream)

higher compared to *PSA-Only* case. In addition, it can be noted that as the CO_2 content increases the optimal purge-to-feed ratio increases too, for all configurations. This can be explained by the fact that more gas is needed to purge beds when the amount of impurities is higher. Only two points are exceptions, C1–3 % CO_2 and C2–3 % CO_2, which may be attributed to the numerical issues.

4.1.5 Membrane properties

The optimal membrane area, membrane thickness and support thickness in *Mem-PSA* case for all configurations and different CO_2 contents in the membrane outlet stream are given in Figs. 11, 12, and 13, respectively. It can be observed that when a higher CO_2 content is allowed to leave the membrane unit - the membrane area is lower, membrane thickness increases as the allowed CO_2 content increases, and the support thickness decreases as the allowed CO_2 content increases.

The membrane stage-cut, fraction of feed permeated through a membrane, in *Mem-PSA* case is presented in Table 4. Quite low values have been observed: 0.15–0.22. This is in agreement with the objective of maximizing hydrogen recovery, effectively demanding the minimal losses through a membrane. Therefore, low membrane stage-cut values are expected and desirable.

4.1.6 Waste gases

The averaged waste gas compositions in *PSA-Only* case for all configurations is given in Table 5, while the averaged waste gas compositions after PSA unit and the retentate/

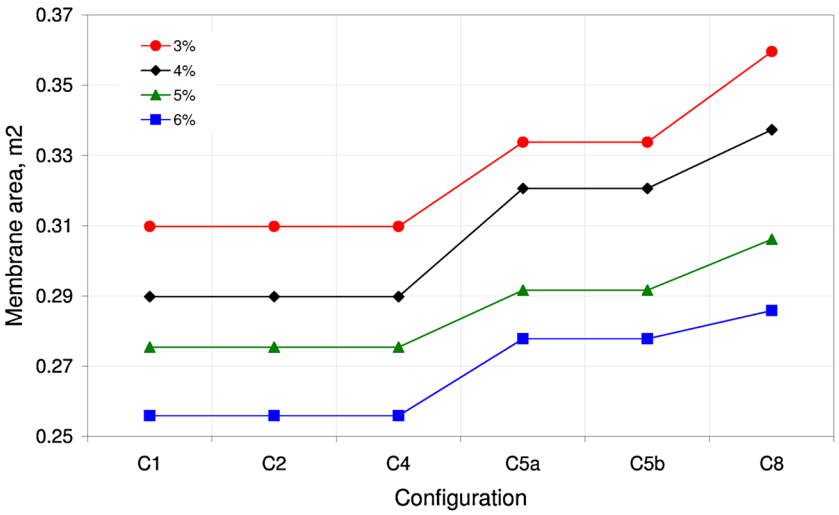

Fig. 11 Optimal values of membrane area in *Mem-PSA* case (for all configurations and different CO_2 contents in the membrane retentate stream)

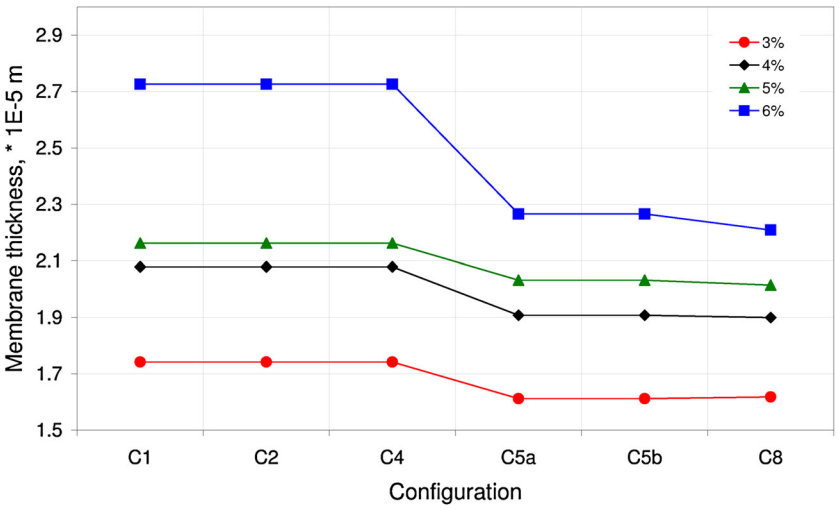

Fig. 12 Optimal values of membrane thickness in *Mem-PSA* case (for all configurations and different CO_2 contents in the membrane retentate stream)

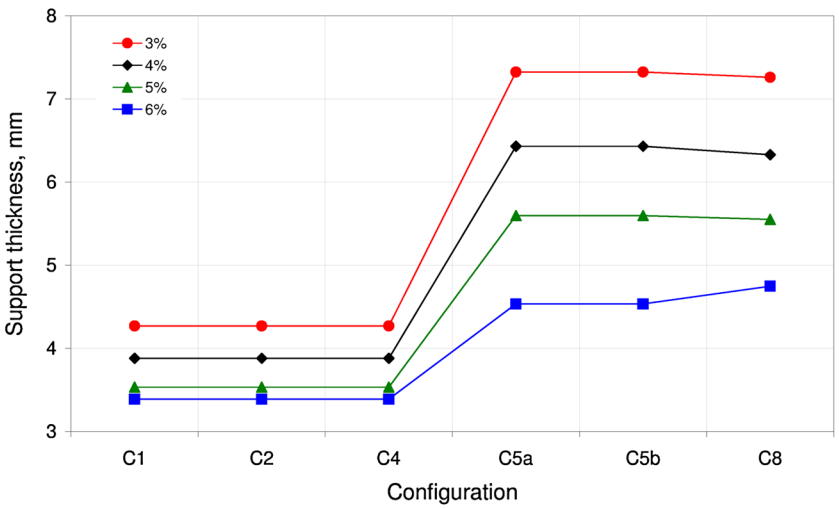

Fig. 13 Optimal values of support thickness in *Mem-PSA* case (for all configurations and different CO_2 contents in the membrane retentate stream)

Table 4 Membrane stage-cut in *Mem-PSA* case (for different CO_2 contents in the membrane retentate stream)

Config.	3 %	4 %	5 %	6 %
C1	0.2174	0.1928	0.1728	0.1554
C2	0.2174	0.1928	0.1728	0.1554
C4	0.2174	0.1928	0.1728	0.1554
C5a	0.2091	0.1904	0.1712	0.1542
C5b	0.2091	0.1904	0.1712	0.1542
C8	0.2083	0.1897	0.1708	0.1538

Table 5 Averaged waste gas compositions after PSA unit in *PSA-Only* case

Config.	H_2	CO	CH_4	CO_2
C1	0.446328	0.091633	0.079067	0.382972
C2	0.391365	0.101102	0.086686	0.420847
C4	0.324356	0.115205	0.088491	0.471948
C5a	0.393019	0.101880	0.086310	0.418792
C5b	0.272536	0.112716	0.105122	0.509626
C8	0.306308	0.100415	0.100376	0.492901

Table 6 Averaged waste gas compositions after PSA unit in *Mem-PSA* case (for all configurations and $x_{CO_2} = 3\ \%$ in the membrane retentate stream)

Config.	H_2	CO	CH_4	CO_2
C1	0.73699	0.09005	0.07400	0.09897
C2	0.70340	0.10036	0.08285	0.11340
C4	0.60199	0.13576	0.11055	0.15170
C5a	0.68489	0.10962	0.08663	0.11885
C5b	0.56268	0.15125	0.12426	0.16181
C8	0.63256	0.12672	0.10505	0.13567

permeate compositions in *Mem-PSA* case, for all configurations and CO_2 content of 3 % in membrane retentate are shown in Tables 6 and 7, respectively. It can be observed that by employing this hybrid scheme it is possible achieve up to 106 % higher H_2 content and up to 74 % lower CO_2 content in waste gases compared to *PSA-Only* case, the concentration of $H_2 + CH_4$ combined in the waste gases from the PSA unit is 81–74 % compared to just 53–41 % in *PSA-Only*. Also, the concentration of the $CO + CO_2$ stream in the membrane permeate is 73–76 %.

4.2 Case 2: *PSA-Mem*

As it was emphasized previously, the optimization results of the first problem in this case study are identical to the results in the *PSA-Only* case. The optimization results of the second problem, which involves the optimization of the membrane, are presented in Table 8. The results show that the major part of CO and CO_2 can be removed from the waste gases (the concentration of H_2 and CH_4 combined is between 95 and 96.7 %). However, the retentate flowrate is rather low, compared to the feed flow rate, and it is only a small fraction of it, 8–23 %. This can be seen from the values of the stage-cut (θ_m) shown in Table 8. Note that membrane stage cut is defined as the ratio of the permeate flow rate over fed flow rate, so it is expected that this value will increase as the ratio of retentate over feed flow rate decreases. Moreover, from Table 9, where the membrane retentate/permeate compositions are given for all configurations, we can see that the concentration of $CO + CO_2$ combined in the permeate stream is of a moderate purity (53–65 %) and not suitable for immediate sequestration but must be further processed. Also, the operating costs, mainly the power requirements, are higher because of the use of the compressor.

4.3 Case 3: *Mem-PSA-Mem*

Again, the optimization results of the first problem in this case study are identical to the optimization results in *Mem-PSA* case. Comparison of the combined H_2 and CH_4 content in the retentate stream of the second membrane in *Mem-PSA-Mem* case for all configurations and different CO_2 contents in the retentate stream of the first membrane is given in Fig. 14. Comparisons of the area, the thickness and the support thickness of the second membrane in *Mem-PSA-Mem* case, for all configurations and different CO_2 contents in the retentate stream of the first membrane are presented in Figs. 15, 16 and 17, respectively. The membrane optimization results of the second problem in *Mem-PSA-Mem* case, for all configurations and $x_{CO_2} = 3\ \%$ in the retentate of the first membrane, are presented in Table 10.

The results in Fig. 14 show again that the major part of CO and CO_2 can be removed from the waste gases (the concentration of H_2 and CH_4 combined is between 95.5 and 97.5 %). However, the ratio of retentate over feed flow rate is again rather low: 9–22 % (see also stage-cut Table 10). Moreover, H_2 concentration in the permeate stream is rather high, 46–69 %, while the concentration of $CO + CO_2$ combined in the permeate stream produced by the second membrane is very low and a possible solution would be to recycle it back to the process to mix it with the fresh feed. The operating costs are again higher because of the use of a compressor.

5 Conclusions

A mathematical framework for modelling and optimization of hybrid PSA/porous membrane gas separation units has been proposed, developed and applied to the case of

Table 7 Membrane retentate/permeate compositions in *Mem-PSA* case (for all configurations and $x_{CO_2} = 3$ % in the membrane retentate stream)

Config.	Retentate molar fractions				Permeate molar fractions			
	H_2	CO	CH_4	CO_2	H_2	CO	CH_4	CO_2
C1	0.92108	0.02682	0.02210	0.03000	0.18894	0.09048	0.08405	0.63654
C2	0.92108	0.02682	0.02210	0.03000	0.18894	0.09048	0.08405	0.63654
C4	0.92108	0.02682	0.02210	0.03000	0.18894	0.09048	0.08405	0.63654
C5a	0.91743	0.02881	0.02377	0.03000	0.16522	0.08622	0.08095	0.66761
C5b	0.91743	0.02881	0.02377	0.03000	0.16522	0.08622	0.08095	0.66761
C8	0.91715	0.02895	0.02390	0.03000	0.16072	0.08582	0.08057	0.67288

Table 8 The membrane optimization results in *PSA-Mem* case (for all configurations)

Config.	A_{memb} (m^2)	δ_{memb} ($\times 10^5$ m)	P_{feed} (bar)	δ_{supp} (mm)	$x_{(H_2)+(CH_4)}$ (%)	θ_m
C1	0.2219	0.6842	12.3153	3.6075	96.7748	0.8875
C2	0.2120	0.6760	12.4800	4.2400	96.3464	0.8602
C4	0.3449	0.8515	12.3112	4.8801	96.1100	0.9044
C5a	0.2081	0.6838	12.3241	4.1621	95.4681	0.7668
C5b	0.3194	0.9263	12.4916	4.6424	95.0343	0.8685
C8	0.2127	0.6747	12.5066	4.2533	96.0255	0.9162

Table 9 Membrane retentate/permeate compositions in *PSA-Mem* case

Config.	Retentate molar fractions				Permeate molar fractions			
	H_2	CO	CH_4	CO_2	H_2	CO	CH_4	CO_2
C1	0.95549	0.01620	0.01226	0.01606	0.37992	0.10090	0.08731	0.43187
C2	0.94700	0.02144	0.01583	0.01509	0.29993	0.11351	0.09777	0.48880
C4	0.94510	0.02442	0.01600	0.01448	0.25831	0.12406	0.09562	0.52201
C5a	0.93339	0.02856	0.02076	0.01676	0.22838	0.12352	0.10571	0.54240
C5b	0.92464	0.03310	0.02575	0.01656	0.17448	0.12398	0.11644	0.58510
C8	0.94075	0.02301	0.01950	0.01674	0.24805	0.10692	0.10723	0.53779

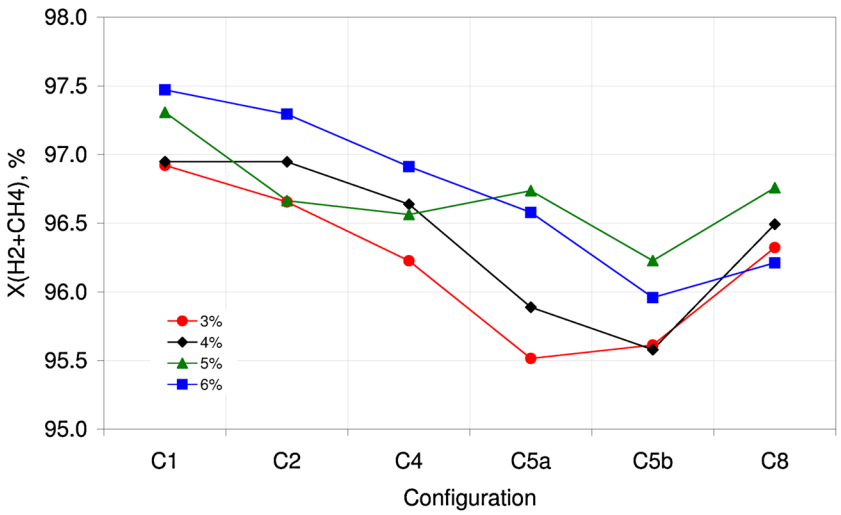

Fig. 14 Combined H_2 and CH_4 content in the retentate stream of the second membrane in *Mem-PSA-Mem* case (for all configurations and different CO_2 contents in the retentate stream of the first membrane)

hydrogen production from SMROG. Several hybrid separation schemes have been analyzed and possibilities for process improvement are discussed and critically assessed. Three distinct hybrid configurations have been studied: CO_2 selective membrane attached to feed stream (*Mem-PSA*), CO_2 selective membrane attached to waste gas streams (*PSA-Mem*) and CO_2 selective membranes attached to both feed and waste gases streams (*Mem-PSA-Mem*).

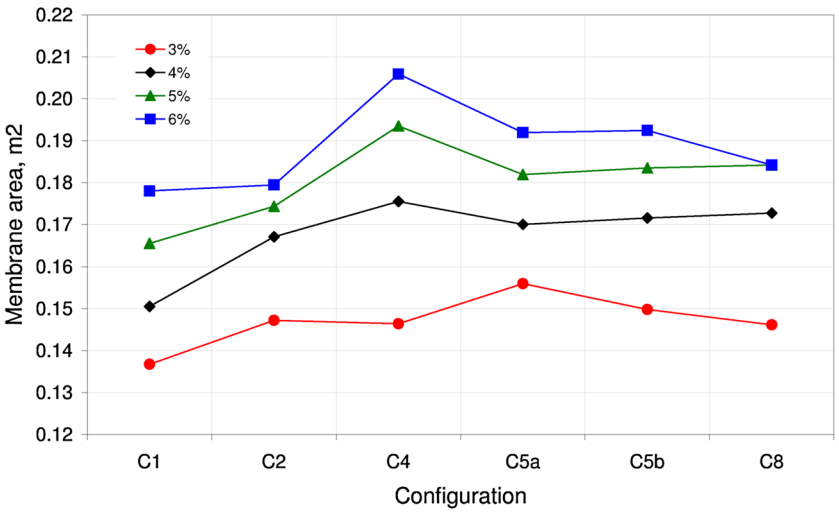

Fig. 15 Optimal values of the area of the second membrane in *Mem-PSA-Mem* case (for all configurations and different CO_2 contents in the retentate stream of the first membrane)

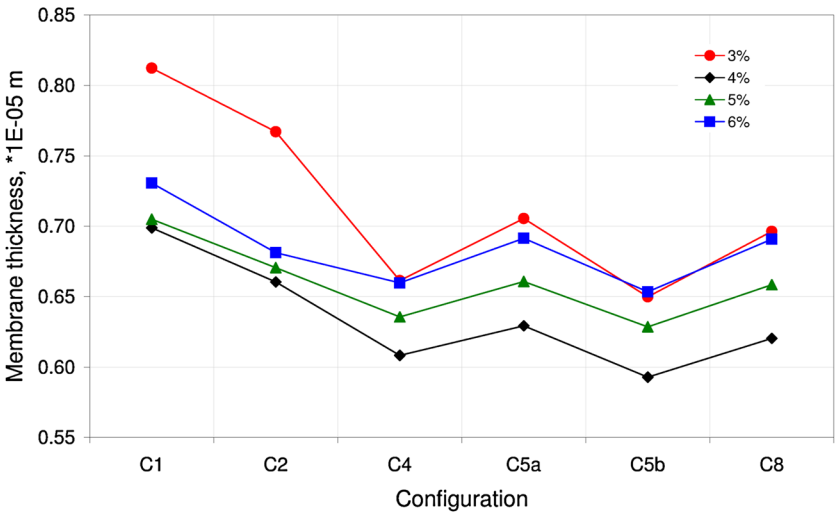

Fig. 16 Optimal values of the thickness of the second membrane in *Mem-PSA-Mem* case (for all configurations and different CO_2 contents in the retentate stream of the first membrane)

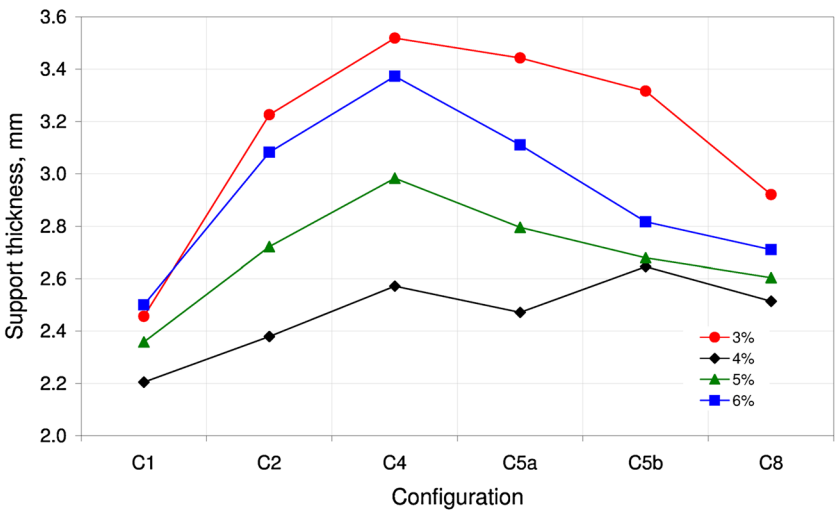

Fig. 17 Optimal values of the support thickness of the second membrane in *Mem-PSA-Mem* case (for all configurations and different CO_2 contents in the retentate stream of the first membrane)

Table 10 The optimization results of the second membrane in *Mem-PSA-Mem* case (for $x_{CO_2} = 3\ \%$ in the retentate stream of the first membrane)

Config.	A_{memb} (m^2)	δ_{memb} ($\times 10^5$ m)	P_{feed} (bar)	δ_{supp} (mm)	$x_{(H_2)+(CH_4)}$ (%)	θ_m
C1	0.1367	0.8122	6.4362	2.4560	96.9210	0.8203
C2	0.1472	0.7671	6.8611	3.2252	96.6542	0.7824
C4	0.1464	0.6613	7.4080	3.5186	96.2252	0.8409
C5a	0.1559	0.7054	7.1418	3.4428	95.5145	0.9132
C5b	0.1498	0.6499	7.5875	3.3159	95.6123	0.7839
C8	0.1462	0.6963	7.1447	2.9203	96.3220	0.8928

The overall hydrogen recovery for given minimum requirements in product purity has been systematically maximized using recent advances on process optimization while optimizing the number of beds, PSA cycle configuration and various PSA and membrane operating and design parameters. The optimization results have been compared to the optimization results of the PSA only case. Benefits from the hybrid gas separation systems have been assessed in terms of the improvements in the overall hydrogen recovery, reduction of adsorption beds size, concentration of the carbon dioxide and carbon monoxide captured in a separate stream, and reduction of the carbon dioxide content in the waste gas streams. The major improvements include: increase in the overall hydrogen recovery ($\sim$2 %), significant reduction in bed size (up to 46 %) that is increase in adsorbent productivity (up to 184 %), concentration of the captured carbon monoxide and carbon dioxide (up to 76 % of carbon monoxide and carbon dioxide combined). Since the accurate techno-economical parameters of the process are not available it was not possible to asses whether the obtained improvements are large enough to overcome the required capital and extra operating costs.

Acknowledgments Financial support from PRISM EC-funded RTN (Contract number MRTN-CT-2004-512233) is gratefully acknowledged.

References

Baker, R.W.: Future directions of membrane gas separation technology. Ind. Eng. Chem. Res. **41**, 1393–1411 (2002)

Bakker, W.J.W., van den Broeke, L.J.P., Kapteijn, F., Moulijn, J.A.: Temperature dependence of one-component permeation through a Silicalite-1 membrane. AIChE J. **43**, 2203–2214 (1997)

Chen, Y.D., Yang, R.T.: Predicting binary Fickian diffusivities from pure-component Fickian diffusivities for surface diffusion. Chem. Eng. Sci. **47**, 3895–3905 (1992)

Esteves, I.A.A.C., Mota, J.P.B.: Simulation of a new hybrid membrane/pressure swing adsorption process for gas separation. Desalination **148**, 275–280 (2002)

Esteves, I.A.A.C., Mota, J.P.B.: Gas separation by a novel hybrid membrane/pressure swing adsorption process. Ind. Eng. Chem. Res. **46**, 5723–5733 (2007)

Farooq, S., Ruthven, D.M.: Numerical simulation of a pressure swing adsorption oxygen unit. Chem. Eng. Sci. **44**, 2809 (1989)

Feng, X., Pan, C.Y., Ivory, J., Ghosh, D.: Integrated membrane/adsorption process for gas separation. Chem. Eng. Sci. **53**, 1689–1698 (1998)

Grol, E.: Integration of H_2 separation membranes with CO_2 capture and compression. DOE/NETL-401/113009 Report. http://www.netl.doe.gov/energy-analyses/pubs/H2_Mmbrn_Assmnt.pdf (2009). Accessed Online 1 July 2013

Kapteijn, F., Moulijn, J.A., Krishna, R.: The generalized Maxwell-Stefan model for diffusion in zeolites: sorbate molecules with different saturation loadings. Chem. Eng. Sci. **55**, 2923–2930 (2000)

Kärger, J., Bülow, M.: Theoretical prediction of uptake behaviour in adsorption kinetics of binary gas mixtures using irreversible thermodynamics. Chem. Eng. Sci. **30**, 893 (1975)

Kärger, J., Ruthven, D.M.: Diffusion in Zeolites and Other Microporous Solids. Wiley, New York (1992)

Krishna, R.: A unified theory of separation processes based on irreversible thermodynamics. Chem. Eng. Commun. **59**, 33–64 (1987)

Krishna, R.: Multicomponent surface diffusion of adsorbed species. A description based on the generalized Maxwell-Stefan diffusion equations. Chem. Eng. Sci. **45**, 1779–1791 (1990)

Krishna, R.: A unified approach to the modeling of intraparticle diffusion in adsorption processes. Gas Sep. Purif. **7**, 91–104 (1993)

Krishna, R., Baur, R.: Modelling issues in zeolite based separation processes. Sep. Purif. Technol. **33**, 213–254 (2003)

Krishna, R., van Baten, J.M.: Diffusion of alkane mixtures in zeolites. Validating the Maxwell-Stefan formulation using MD simulations. J. Phys. Chem. **109**, 6386 (2005a)

Krishna, R., van Baten, J.M.: Kinetic Monte Carlo simulations of the loading dependence of diffusion in zeolites. Chem. Eng. Technol. **28**, 160 (2005b)

Krishna, R., van Baten, J.M.: Linking the loading dependence of the Maxwell-Stefan diffusivity of linear alkanes in zeolites with the thermodynamic correction factor. Chem. Phys. Lett. **420**, 545–549 (2006)

Krishna, R., van den Broeke, L.J.P.: The Maxwell-Stefan description of mass transport across zeolite membranes. Chem. Eng. J. **57**, 155–162 (1995)

Krishna, R., Wesselingh, J.A.: The Maxwell-Stefan approach to mass transfer. Chem. Eng. Sci. **52**, 861–911 (1997)

Krishna, R., Paschek, D.: Separation of hydrocarbon mixtures using zeolite membranes: a modelling approach combining molecular simulations with the Maxwell-Stefan theory. Sep. Purif. Technol. **21**, 111–136 (2000)

Krishna, R., Paschek, D., Baur, R.: Modelling the occupancy dependence of diffusivities in zeolites. Microporous Mesoporous Mater. **76**, 233 (2004)

Krishna, R., van Baten, J.M., Garcıa-Perez, E., Calero, S.: Incorporating the loading dependence of the Maxwell-Stefan diffusivity in the modeling of CH4 and CO2 permeation across zeolite membranes. Ind. Eng. Chem. Res. **46**, 2974–2986 (2007)

Mercea, P., Hwang, S.T.: Oxygen separation from air by a combined pressure swing adsorption and continuous membrane column process. J. Memb. Sci. **88**, 132 (1994)

Nikolic, D., Giovanoglou, A., Georgiadis, M.C., Kikkinides, E.S.: Generic modeling framework for gas separations using multibed pressure swing adsorption processes. Ind. Eng. Chem. Res. **47**, 3156–3169 (2008)

Nikolic, D., Kikkinides, E.S., Georgiadis, M.C.: Optimization of multibed PSA processes. Ind. Eng. Chem. Res. **48**, 5388–5398 (2009)

Process Systems Enterprise Ltd.: http://www.psenterprise.com. (2011)

Ritter, J.A., Ebner, A.D.: State-of-the-art adsorption and membrane separation processes for hydrogen production in the chemical and petrochemical industries. Sep. Sci. Technol. **42**, 1123–1193 (2007)

Ruthven, D.M.: Principles of Adsorption and Adsorption Processes. Wiley, New York (1984)

Ruthven, D.M.: PSA vs membrane processes for gas separation. Membr. Q. **9**, 3, 7 (1994)

Sikavitsas, V.I., Yang, R.T.: Predicting multicomponent diffusivities for diffusion on surfaces and in molecular sieves with energy heterogeneity. Chem. Eng. Sci. **50**, 3057 (1995)

Sircar, S., Waldron, W.E., Rao, M.B., Anand, M.: Hydrogen production by hybrid SMR–PSA–SSF membrane system. Sep. Purif. Technol. **17**, 11–20 (1999)

Van de Graaf, J.M., Kapteijn, F., Moulijn, J.A.: Modeling permeation of binary mixtures through zeolite membranes. AIChE J. **45**, 497–511 (1999)

Van de Graaf, J.M., Kapteijn, F., Moulijn, J.A.: Diffusivities of light alkanes in a silicalite-1 membrane layer. Microporous Mesoporous Mater. **35**, 267–281 (2000)

Van den Broeke, L.J.P., Krishna, R.: Experimental verification of the Maxwell-Stefan theory for micropore diffusion. Chem. Eng. Sci. **50**, 2507–2522 (1995)

Vareltzis, P., Kikkinides, E.S., Georgiadis, M.C.: On the optimization of gas separation processes using zeolite membranes. Trans. IChemE **81**, 525–536 (2003)

Yang, R.T.: Gas Separation by Adsorption Processes. Butterworths, Boston (1987)

Yang, R.T., Fenn, J.B., Haller, G.L.: Modification to the Higashi model for surface diffusion. AIChE J. **19**, 1052–1053 (1973)

Zolandz, R.R., Fleming, G.K.: Gas permeation. In: Ho, W.S.W., Sirkar, K.K. (eds.) Membrane Handbook. Van Nostrand Reinhold, New York (1992)